Case Studies in Thermal Engineering 50 (2023) 103406

Contents lists available at ScienceDirect

Case Studies in Thermal Engineering

journal homepage: www.elsevier.com/locate/csite

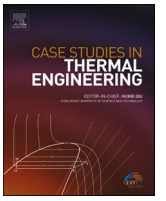

Theoretical exploration of heat transport in a stagnant power-law fluid flow over a stretching spinning porous disk filled with homogeneous-heterogeneous chemical reactions

Zhihong He [a], Muhammad Bilal Arain [b,**], Usman [c,*], W.A. Khan [d], Ali Rashash R Alzahrani [e], Taseer Muhammad [f], A.S. Hendy [g], Mohamed R. Ali [h,i]

[a] School of Mathematics and Information Sciences,Yantai University, Yantai 264005, China
[b] State Key Laboratory of Mechanics and Control of Mechanical Structures, Nanjing University of Aeronautics and Astronautics, Nanjing 210016, People's Republic of China
[c] Department of Computer Science, National University of Sciences and Technology, Balochistan Campus (NBC), Quetta, 87300, Pakistan
[d] Department of Mechanical Engineering, College of Engineering, Prince Mohammad Bin Fahd University, Al Khobar 31952, Saudi Arabia
[e] College of Applied Sciences, Department of Mathematical Sciences, Umm Al-Qura University, Makkah, 24382, Saudi Arabia
[f] Department of Mathematics, College of Sciences, King Khalid University, Abha, 61413, Saudi Arabia
[g] Department of Computational Mathematics and Computer Science, Institute of Natural Sciences and Mathematics, Ural Federal University, 19 Mira St., Yekaterinburg 620002, Russia
[h] Basic Engineering Science Department, Benha Faculty of Engineering, Benha University, Benha, Egypt
[i] Faculty of Engineering and Technology, Future University in Egypt, New Cairo, 11835, Egypt

ARTICLE INFO

Handling Editor: Huihe Qiu

Keywords:
Homogeneous-heterogeneous reactions
Power-law fluids
Porous disk
Stagnant flow

ABSTRACT

The distinction between homogeneous and heterogeneous chemical reactions is crucial because many chemically reactive systems, such as hydrometallurgical processes, cooling towers, biological systems, fog dispersion, catalysis, etc., involve both types of reactions. Thus, this study analyzes the heat transmission (HT) characteristics in an MHD stagnant flow of power-law fluid caused by a spinning disk that is stretched and saturated in a porous medium. The study considers homogeneous-heterogeneous (HH) reactions and nonlinear thermal radiation subject to no-slip and convection boundary conditions. The leading equations are switched into ordinary differential equations (ODEs) employing similarity variables. The study focuses on the dimensionless concentration, velocity, temperature, Nusselt number, and skin friction coefficient, which are discussed in detail in the results and discussion section. The study observes that for power-law fluids with an index value less than 1, the skin friction coefficient decays as the power-law index grows. It also notes that the dimensionless skin friction of power-law fluids decreases as the velocity ratio increases. The dimensionless concentration increases with Schmidt and modified Prandtl numbers for both power-law fluids over a stretching spinning porous disk. The HH reaction parameters decline the concentration of power-law fluids.

* Corresponding author.
** Corresponding author. State Key Laboratory of Mechanics and Control of Mechanical Structures, Nanjing University of Aeronautics and Astronautics, Nanjing 210016, People's Republic of China.
E-mail addresses: mbarain@nuaa.edu.cn (M.B. Arain), usman.malik.ms@gmail.com (Usman).

https://doi.org/10.1016/j.csite.2023.103406
Received 10 June 2023; Received in revised form 9 August 2023; Accepted 20 August 2023
Available online 25 August 2023

Nomenclature

A, B	Chemical species
$\varphi_A(\eta)$, $\varphi_B(\eta)$	Reduced concentrations of chemical species A and B
D_A, D_B	Diffusion constants of A and B
$F(\eta), G(\eta)$, $H(\eta)$	Reduced radial, azimuthal and axial velocities
u_e, v_e	Free stream velocities
B_0	Magnetic field strength
ρ	Density*(M/L^3)*
T	Temperature*(K)*
k	Thermal conductivity*(W/m-k)*
c	Constant rate
h_1	Heat transfer coefficient
τ_{rz}, $\tau_{\theta^* z}$	Radial and azimuthal directions shear stress
a_∞	Ambient concentration
θ	Dimensionless temperature
ω	Rotation parameter
λ	Velocity Ratio Parameter
K_p	Permeability Parameter
Rd	Radiation Parameter*(W/m^2)*
Pr_m	Modified Prandtl Number
K_1	Homogeneous Reaction Parameter
$C_{G\theta^*}$	Azimuthal direction skin friction
q_w	Heat flux (W/m^2)
a, b	Concentrations of chemical species A and B
k_C, k_S	Rate constants
u, v, w	Velocity components *(L/T)*
r, θ^*, z	Cylindrical coordinates *(L)*
σ	Electrical diffusivity
μ	Dynamic viscosity
k_p^*	Permeability of porosity
c_p	Specific heat
q_r	Heat flux*(W/m^2)*
Ω	Angular velocity
T_w	Surface temperature
T_∞	Ambient temperature *(K)*
η	Similarity variable
n	Power-law index
C_{Fr}	Radial direction skin friction
M	Magnetic Parameter
Pr	Prandtl Number(−)
θ_w	Surface Heating Parameter
Sc	Schmidt Number(−)
δ	Diffusion Ratio Parameter*(L^2/T)*
K_2	Heterogeneous Reaction Parameter
Nu_r	Local Nusselt number(−)
Re_r	Local Reynold's number(−)

1. Introduction

Stagnant point flow refers to the flow of a fluid (liquid or gas) around a solid object where the fluid velocity is zero at a specific point on the surface of the object. This point is termed the stagnant point. The stagnant point is typically found on the leading edge of a solid object, where the fluid is forced to split into two streams as it flows around the object. As the fluid streams converge at the stagnation point, their velocities are reduced to zero, and the pressure in the fluid increases. The fluid then flows away from the stagnant point, around the object, and eventually rejoins downstream of the object. Stagnant point flow has important applications in fluid mechanics, particularly in the study of aerodynamics. The flow around airfoils, such as wings on an aircraft, is an example of stagnant point flow.

The behavior of the fluid at the stagnant point can have a significant impact on the aerodynamic forces acting on the object, including lift and drag. Engineers use knowledge of stagnant point flow to design more efficient and effective aerodynamic shapes for aircraft, rockets, and other objects that move through fluids.

Several essential applied fluids, like molten plastic, polymers, food, slurries, and many others, have non-Newtonian flow characteristics. Because of the escalating usage of these non-Newtonian polymers in many manufacturing and processing industries, significant attempts have been made to better understand their friction and HT properties. The empirical Ostwald-de Waele model [1], often known as the power-law viscosity model, predicts that shear stress changes as a power function of strain rate in many non-Newtonian inelastic fluids found in chemical engineering processes and the biochemical industry. Studying diverse fluid mechanics and HT phenomena, however, requires taking into account extra factors since such fluids have more complex equations than Newtonian fluids that link shear stress to velocity fields. Mustafa et al. [2] investigated the nonlinear radiation HT problem for non-Newtonian fluid stagnant point flow using the power-law model. Usman et al. [3] studied the time-independent movement of the power-law nanofluid between stretching rotatable disks. The flow of a constant transverse magnetic field through a power-law fluid that conducts electricity was studied by Cortell [4].

The flow of fluids resulting from a disc rotation issue is crucial in industrial and engineering uses, including those involving computer storage devices, electrical devices, rotatable machinery, the petroleum sector, MHD rotators, medical apparatus, and many more. In the domains of aeronautical engineering and construction, rotating disc flow plays a key role in things like gas turbine rotors, heated power production frameworks, air cleaning devices, and pivoting machinery. In 1921, the scientist Von Karman [5] looked into the flowing fluid issue in a revolving disk and their numerical solution was presented by Cochran [6]. Stretching transformations, developed by Von Karman, are frequently used to change a set of PDEs into ODEs. Some other studies can be found in Refs. [7–10].

In a stagnant point flow, the fluid flows towards a solid surface and comes to a stop, resulting in a stagnant point. If the flow is rotating, the stagnant point can experience a swirling motion around the axis of rotation. This rotating flow in stagnant point flow is called a vortex. The vortex can be either clockwise or counterclockwise, depending on the direction of rotation. The direction of the vortex is determined by the Coriolis effect, which is a consequence of the rotation of the Earth. The vortex can have a significant effect on the flow around the stagnant point. It can create a region of low pressure at the center of the vortex, which can cause the fluid to flow away from the surface. This effect is known as the Magnus effect, and it is responsible for the curving motion of a spinning ball in flight. Millsaps and Pohlhausen [11] examine an accurate solution to the HT issue for the von Karman case of laminar viscous fluid flow upon a rotatable plate. Shamshuddin et al. [12] carried out a numerically handled movement of a micropolar nanofluid through a porous stretchable surface. Analysis of non-Newtonian visco-inelastic fluid flow concerning two discs was covered by Reshu Agarwal et al. [13]. A 3D magneto stagnant-point flow of tri-hybrid nanofluid was explored by Gupta and Rana [14] using an infinite gyrating disc that is radially stretched and has many slip influences. Vijay and Sharma [15] investigated the MHD rotational stagnant point flow of a temperature-dependent viscous Maxwell nanofluid concerning a radially extending rotatable disk.

Homogeneous reactions are chemical reactions that occur between substances in the same phase, typically either all gases, all liquids, or all solids. In a homogeneous reaction, the products and reactants are in a similar phase. Heterogeneous reactions, on the other hand, are chemical reactions that occur between substances in different phases, typically between a solid and a gas, a solid and a liquid, or a liquid and a gas. Heterogeneous reactions often involve a solid catalyst, which can speed up the reaction by providing a surface for the reactant molecules to come into contact with each other. Homogeneous reactions, on the other hand, typically do not involve a catalyst, as the reactants are already in close proximity to each other in the same phase. The stagnant point Casson fluid flow concerning a stretchable sheet was deliberated by Khan et al. [16] using magnetohydrodynamic (MHD). Gholinia et al. [17] research focuses on the Eyring-Powell nanofluid flow feature caused by spinning disk with a variety of physical forces, including MHD, slip flow, and HH reactions. The stretched flow of viscoelastic fluid with curved sheet in two dimensions is scrutinized by Imtiaz et al. [18]. Sreedevi et al. [19] inspected the impact of HH reactions on the flow, mass, and HT analyses of a Tiwari-Das type Maxwell nanofluid upon a stretchable cylinder. In their study, Khan and Pop [20] investigated how steady viscoelastic fluids behave when subjected to HH reactions while being stretched on a sheet. They utilized the Chaudhary and Merkin model and observed that the viscoelastic parameter had a negative effect on surface concentration. In contrast, the power of homogeneous reactions had a positive effect, and heterogeneous reactions further intensified this effect. Bachok et al. [21] investigated how HH reactions affected the time-independent boundary layer flow (BLF) close to the stagnant point on a stretchable surface. They experienced that a boundary layer (BL) is shaped in a fluid with low kinematic viscosity when the stretchable velocity is lower than the free stream velocity. Conversely, an inverted BL is shaped when the stretchable velocity surpasses the free stream velocity. The impressions of HH reactions in nanofluid flow upon a stretchable sheet put in a permeable media soaked with a nanofluid were analyzed by Kameswaran and colleagues [22]. Their findings revealed that the Cu-water nanofluid exhibited greater levels of reduced skin friction and HT likened to other nanofluids. In their study, Shaw and co-authors [23] investigated how a HH reaction impacts the time-independent flow of micropolar fluid from a shrinking/stretching sheet. They discovered that the solute surface concentration decays with the strength of homogeneous reactions but increases with the permeability parameter, heterogeneous reactions, and shrinking/stretching parameters. Additionally, the surface velocity was observed to escalate with the micropolar parameter. The impact of HH reactions on an MHD viscous fluid close to the stagnant point passing a shrinking/stretching sheet with generalized slip condition and uniform suction was examined by Abbas and colleagues [24]. Their findings indicated that, for a shrinking sheet, two solutions occur within a particular span of parameters, while for a stretchable sheet, only one solution is present.

Sheikh and Abbas [25] investigated the impact of HH reaction on the BLF of a Casson fluid close to a stagnant point upon a porous shrinking/stretchable sheet with a constant suction. They discovered that an escalation in the fluid velocity slip parameter causes a reduction in velocity magnitude and a rise in concentration within the BL region. Hayat and colleagues [26] studied the stagnant flow of a 3rd-grade fluid past a stretchable sheet with variable thickness and assumed the impressions of HH reactions. Their findings

indicated that the temperature and velocity fields escalate as the shape parameter increases. Additionally, boosting estimations of the homogeneous parameter result in a weakening in the concentration outline. Furthermore, the velocity outline is enhanced when the relation of free stream and stretchable velocities and wall thickness parameter is escalated. Jain and Gupta [27] investigated water-based CNTs' nanofluid flow upon an inclined 3D nonlinear stretchable sheet with HH reactions in a porous medium. They found similar impacts of HH reaction parameters on the concentration profile field. Anuar and co-authors [28] investigated the time-independent 2D stagnant flow of nanofluids upon an exponentially shrinking/stretchable sheet with HH reactions. Their analysis revealed that dual solutions occur for an exponentially shrinkable sheet. Furthermore, they found that the 1st solutions are stable, while the 2nd solutions are unstable based on their results. A boundary-layer flow model for homogeneous-heterogeneous reactions is offered Merkin [29]. Some other related references are listed in Refs. [30–32].

From the above-mentioned literature, it is revealed that no investigation is done on HT in a Power-Law Stagnation Fluid Flow over a stretchable spinning porous disk along with HH reactions. The leading PDEs are transmuted to ODEs and then handled with the computational software MAPLE, and the results are shown in tabular and graphical form. Physically interesting quantities are also calculated for the purpose of engineering applications.

2. Mathematical formulation

A stagnant time-independent incompressible 3D flow of an MHD power-law fluid on a stretchable rotatable porous disk filled with HH chemical reactions is examined, as shown in Fig. 1. The components of the velocity u, v, w are selected along cylindrical coordinates system r, θ^*, z. The disc rotates alongside the z-axis with regard to both angular velocity and a constant. The disc stretches radially with a velocity of $u = cr$, where c is a constant. Axial flow prevents consideration of the variation in θ^* direction. The constant magnetic field retains a power of B_0 is functioned vertically in the $z-$ direction. The pressure is viewed as constant over the whole BL. The free stream velocity $u_e = \varepsilon r$ that is away from the BL is labeled as the potential flow. The disk is kept at and away from the surface with constant temperatures T_w and T_∞. Also, the convective HT mechanism with nonlinearized thermal radiation is investigated.

HH chemical reactions of species A and B are analyzed through flow analysis. The cubic autocatalysis homogeneous reaction can be formulated in the following manner [22,23]:

$$2B + A \to 3B, \text{rate} = ab^2 k_c, \tag{1}$$

The following format represents the 1st-order isothermal reaction taking place on the catalyst surface.

$$A \to B, \text{rate} = ak_s, \tag{2}$$

The rate constants k_c and k_s are used in the expression where a and b represent the concentrations of chemical species A and B. Both reaction mechanisms are thought to be isothermal. Following these suppositions, the governing equations are as [24,25]:

$$\frac{\partial u}{\partial r} + \frac{u}{r} + \frac{\partial w}{\partial z} = 0 \tag{3}$$

$$u\frac{\partial u}{\partial r} - \frac{v^2}{r} + w\frac{\partial u}{\partial z} = u_e\frac{du_e}{dr} + \frac{1}{\rho}\frac{\partial}{\partial z}\left(\mu\frac{\partial u}{\partial z}\right) - \left(\frac{\sigma B_0^2}{\rho} + \frac{\mu}{\rho k_p^*}\right)(u - u_e) \tag{4}$$

$$u\frac{\partial v}{\partial r} + \frac{uv}{r} + w\frac{\partial v}{\partial z} = \frac{1}{\rho}\frac{\partial}{\partial z}\left(\mu\frac{\partial v}{\partial z}\right) - \left(\frac{\sigma B_0^2}{\rho} + \frac{\mu}{\rho k_p^*}\right)v \tag{5}$$

$$u\frac{\partial T}{\partial r} + w\frac{\partial T}{\partial z} = \frac{1}{\rho c_p}\left\{\frac{\partial}{\partial z}\left(k\frac{\partial T}{\partial z}\right) - \frac{\partial q_r}{\partial z}\right\} \tag{6}$$

$$u\frac{\partial a}{\partial r} + w\frac{\partial a}{\partial z} = D_A\left(\frac{\partial^2 a}{\partial z^2}\right) - k_c ab^2, \tag{7}$$

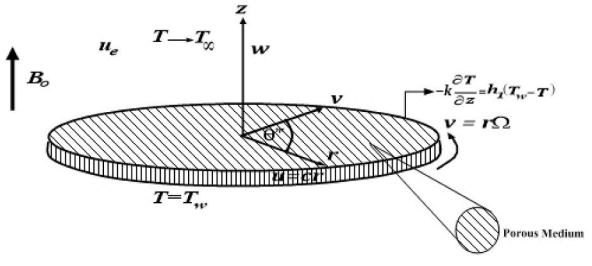

Fig. 1. The flow geometry.

$$u\frac{\partial b}{\partial r}+w\frac{\partial b}{\partial z}=D_B\left(\frac{\partial^2 b}{\partial z^2}\right)+k_c ab^2, \tag{8}$$

Subject to boundary conditions (BCs)

$$u=cr, v=\Omega r, w=0, k\frac{\partial T}{\partial z}=-h_1(T_w-T), D_A\frac{\partial a}{\partial z}=k_s a, D_B\frac{\partial b}{\partial z}=-k_s a \quad \text{at } z=0, \tag{9}$$

$$u=u_e\to\varepsilon r, v=v_e\to 0, w=0, T\to T_\infty, a\to a_\infty, b\to 0, \text{at } z\to\infty \tag{10}$$

Where u, v are the velocity components [3]. The similarity variables for the present problem can be chosen as follows:

$$u=crF(\eta), v=crG(\eta), w=r^{\frac{(n-1)}{(n+1)}}\left(\frac{c^{1-2n}}{\upsilon}\right)^{-\frac{1}{(n+1)}}H(\eta),$$

$$\theta(\eta)=\frac{T-T_\infty}{T_w-T_\infty}, \varphi_A(\eta)=\frac{a}{a_\infty}, \varphi_B(\eta)=\frac{b}{a_\infty}, \eta=zr^{\frac{(1-n)}{(1+n)}}\left(\frac{c^{2-n}}{\upsilon}\right)^{\frac{1}{(n+1)}} \tag{11}$$

After introducing similarity variables, one gets the reduced governing equations as follows:

$$H'=-2F-\frac{1-n}{1+n}\eta F' \tag{12}$$

$$F^2-G^2+\left(\frac{1-n}{1+n}\eta F+H\right)F'=\lambda^2+\left[F'\left\{(G')^2+(F')^2\right\}^{\frac{(n-1)}{2}}\right]'-(M+K_p)(F-\lambda), \tag{13}$$

$$2FG+\left(\frac{1-n}{1+n}\eta F+H\right)G'=\left[G'\left\{(G')^2+(F')^2\right\}^{\frac{(n-1)}{2}}\right]'-(M+K_p)G, \tag{14}$$

$$\left(H+\frac{1-n}{1+n}\eta F\right)\theta'=\frac{1}{Pr}\left[\theta'\left\{1+Rd(1+(\theta_w-1)\theta)^3\right\}\left\{(G')^2+(F')^2\right\}^{\frac{(n-1)}{2}}\right]', \tag{15}$$

$$\varphi_A''-\frac{ScPr_m}{Pr}\left(H+\frac{1-n}{1+n}\eta F\right)\varphi_A'-\frac{ScPr_m}{Pr}K_1\varphi_A{\varphi_B}^2=0, \tag{16}$$

$$\delta\varphi_B''-\frac{ScPr_m}{Pr}\left(H+\frac{1-n}{1+n}\eta F\right)\varphi_B'+\frac{ScPr_m}{Pr}K_1\varphi_A{\varphi_B}^2=0, \tag{17}$$

with transformed BCs

$$G(0)=\omega, F(0)=1, H(0)=0, \theta(0)=1, F(\infty)=\lambda, G(\infty)=0, \theta(\infty)=0 \tag{18}$$

$$\varphi_A'(0)=K_2\varphi_A(0), \delta\varphi_B'(0)=-K_2\varphi_A(0)\varphi_A(\infty)=1, \varphi_B(\infty)=0. \tag{19}$$

where $\varphi_A(\eta)$ and $\varphi_B(\eta)$ signify the dimensionless concentrations of chemical species A and B.

$$\lambda=\frac{\varepsilon}{c}, M=\frac{B_0^2\sigma}{\rho c}, K_p=\frac{\upsilon}{k_p^*}, Pr=\frac{\upsilon}{\alpha}, Rd=\frac{16\sigma^* T_\infty^3}{3kk^*}, \theta_w=\frac{T_w}{T_\infty}, \omega=\frac{\Omega}{c}, Sc=\frac{\upsilon}{D_A},$$
$$Pr_m=\frac{\left(c^3r^2\right)^{\frac{n-1}{n+1}}\upsilon^{\frac{2}{n+1}}}{\alpha}, \delta=\frac{D_B}{D_A}, K_1=\frac{k_c a_\infty^2}{c}, K_2=\frac{k_s}{D_A\left(\frac{c^{2-n}}{\upsilon}\right)^{\frac{1}{n+1}}r^{\frac{1-n}{1+n}}}, \tag{20}$$

The species A and B diffusion coefficients are similar in size. This assumption causes an additional deduction that the diffusion coefficients D_B and D_A are equivalent, represented by $\delta=1$. Therefore, according to Refs. [20,21], we have:

$$\varphi_A+\varphi_B=1 \tag{21}$$

This assumption reduces Eqns. 16 and 17 to

$$\varphi_A''-\frac{Sc\ Pr_m}{Pr}\left(H+\frac{1-n}{1+n}\eta F\right)\varphi_A'+\frac{Sc\ Pr_m}{Pr}K_1\varphi_A(1-\varphi_A)^2=0 \tag{22}$$

With boundary conditions

$$\varphi_A'(0)=K_2\varphi_A(0), \varphi_A(\infty)\to 1 \tag{23}$$

Table 1
Linkage of $F^{'}(0)$, $-G^{'}(0)$, $-H(\infty)$, $-\theta^{'}(0)$ when Pr = 6.2 and $M = 0$ for Newtonian fluids.

	Ref. [35]	Ref. [34]	Ref. [33]	Present Results
$F^{'}(0)$	0.510233	0.5102	0.51023	0.5101
$-G^{'}(0)$	0.615922	0.6159	0.61592	0.6160
$-H(\infty)$	0.884474	–	0.88447	0.8845
$-\theta^{'}(0)$	–	0.9337	0.93388	0.9338

The physically interesting quantities are azimuthal and radial direction skin friction coefficients, and local Nusselt number can be delineated as:

$$C_{G\theta^*} = \frac{\tau_{\theta^* z}}{\rho_f (cr)^2}, C_{Fr} = \frac{\tau_{rz}}{\rho_f (cr)^2}, Nu_r = \frac{rq_w}{k(T_W - T_\infty)}, \tag{24}$$

where

$$\tau_{rz} = \left[\mu\left\{\frac{1}{r}\left(\frac{\partial w}{\partial \theta^*}\right) + \left(\frac{\partial u}{\partial z}\right)\right\}\right]_{z=0} = \left[\mu\left(\frac{\partial u}{\partial z}\right)\right]_{z=0}, \left[\mu\left(\frac{\partial v}{\partial z}\right)\right]_{z=0},$$

$$q_w = \left[-k\frac{\partial T}{\partial z} + (q_r)_w\right]_{z=0} = -\left[\left\{1 + Rd(1 + (\theta_w - 1)\theta)^3\right\}k\frac{\partial T}{\partial z}\right]_{z=0}, \tag{25}$$

So, the dimensionless form can be written as

$$\begin{aligned} &\mathrm{Re}_r^{\frac{1}{n+1}} C_{Fr} = \left[F^{'2}(0) + G^{'2}(0)\right]^{\frac{n-1}{2}} F^{'}(0), \\ &\mathrm{Re}_r^{\frac{1}{n+1}} C_{G\theta^*} = \left[F^{'2}(0) + G^{'2}(0)\right]^{\frac{n-1}{2}} G^{'}(0), \\ &\mathrm{Re}_r^{-\frac{1}{n+1}} Nu_r = -\left[1 + Rd(1 + (\theta_w - 1)\theta(0))^3\right]\theta^{'}(0), \end{aligned} \tag{26}$$

Where, Re_r is the radial Reynolds number

$$\mathrm{Re}_r = \frac{r^2 c^{2-n}}{\nu_f}$$

3. Numerical solution

The Keller-box method (KBM), explained in Refs. [40–42], is used to numerically solve the ODEs subject to BCs for various pertinent parameters. The equations are transformed into a scheme of 1st-order equations and stated in finite difference shapes with central differences. The resulting nonlinear scheme is linearized, benefitting Newton's method, and then put into matrix-vector form. The block-tridiagonal-elimination technique is employed to tackle the resulting linear system together with the BCs. The details of the numerical interpretation can be learned in Ref. [42]. The values of the step size $\Delta\eta$ in η and the location of the edge of the BL η_∞ are controlled for dissimilar parameter values to ensure accurateness. A range of values of $\Delta\eta$ between 0.001 and 0.02 is taken, contingent on the parameters, to obtain mesh-independent numerical values accurateness to at least 4 decimal places. However, for a convergence criterion of 10^{-6}, a uniform grid of $\Delta\eta = 0.01$ is sufficient for precision to 4 decimal places in almost all circumstances. The boundary layer thickness (BLT) η_∞ is chosen 5, where the infinity BC is asymptotically attained.

Tables 1–5 are presented, in the limiting cases, to validate our numerical results with the existing data. It is noted that the outcomes are approximately similar to the previously published articles.

Table 2
Linkage of $F^{'}(0)$ for different non-Newtonian nanofluids when $M = 0, \mathrm{K}_p = 0, \lambda = 0$.

n	Ref. [39]	Ref. [38]	Ref. [37]	Ref. [36]	Present Results
2.5	0.5624	0.56236	–	–	0.5622
2.2	0.5532	0.55319	–	–	0.5531
2	0.5468	0.54676	0.5470	–	0.5467
1.7	0.5366	0.53664	0.5370	–	0.5366
1.5	0.5292	0.52919	0.5290	0.5290	0.52916
1.3	0.5215	0.5215	0.5220	0.5210	0.5221
1	0.5102	0.51021	0.5100	0.5100	0.5102
0.8	0.5038	0.50381	0.5040	0.5040	0.5038
0.5	0.5006	0.50058	0.5010	0.5010	0.5006

Table 3
Linkage of $-G^{'}(0)$ for various non-Newtonian nanofluids when $M=0, K_p=0, \lambda=0$.

n	Ref. [39]	Ref. [38]	Ref. [37]	Ref. [36]	Present Results
2.5	0.6096	0.60967	–	–	0.6097
2.2	0.6057	0.60566	–	–	0.6056
2	0.6033	0.60327	0.603	–	0.6032
1.7	0.6009	0.60091	0.6	–	0.6088
1.5	0.601	0.60099	0.601	0.601	0.6012
1.3	0.6035	0.60346	0.603	0.603	0.6034
1	0.6159	0.61591	0.616	0.616	0.6158
0.8	0.6361	0.63608	0.636	0.636	0.6361
0.5	0.713	0.71322	0.712	0.713	0.7128

Table 4
Linkage of $-H(\infty)$ for different non-Newtonian nanofluids when $M=0, K_p=0, \lambda=0$.

n	Ref. [39]	Ref. [38]	Ref. [37]	Ref. [36]	Present Results
2.5	0.5425	0.5420	–	–	0.5424
2.2	0.5655	0.5655	–	–	0.5655
2	0.5877	0.5876	0.586	–	0.5870
1.7	0.6366	0.6366	0.633	–	0.6334
1.5	0.6783	0.6783	0.676	0.678	0.6781
1.3	0.7359	0.7359	0.735	0.735	0.7360
1	0.8823	0.8823	0.883	–	0.8828
0.8	1.0593	1.0593	1.089	1.052	1.0598

Table 5
Linkage of $-\theta^{'}(0)$ for different non-Newtonian nanofluids when $M=0, K_p=0, \lambda=0$.

n	Ref. [39]	Ref. [38]	Present Results
2.5	0.3996	0.3998	0.3996
2.2	0.3965	0.39655	0.3965
2	0.3939	0.39392	0.3939
1.7	0.3897	0.3897	0.3897
1.5	0.3886	0.38859	0.3886
1.3	0.3891	0.3891	0.3893
1	0.3963	0.39632	0.3963
0.8	0.4111	0.41108	0.4111
0.5	0.4791	0.47917	0.41792

Table 6
Numerical estimations of radial skin friction $\mathrm{Re}_r^{\frac{1}{n+1}}C_{Fr}$, azimuthal skin friction $\mathrm{Re}_r^{\frac{1}{n+1}}C_{G\theta}$ and Nusselt number $\mathrm{Re}_r^{-\frac{1}{n+1}}Nu_r$ for different power-law fluids with $M=1$, $\omega=1, \mathrm{Pr}=1, \theta_w=1.5, Rd=1$.

n	$\mathrm{Re}_r^{\frac{1}{n+1}}C_{Fr}$			$\mathrm{Re}_r^{\frac{1}{n+1}}C_{G\theta}$			$\mathrm{Re}_r^{-\frac{1}{n+1}}Nu_r$		
	$\lambda=0$	$\lambda=0.5$	$\lambda=1$	$\lambda=0$	$\lambda=0.5$	$\lambda=1$	$\lambda=0$	$\lambda=0.5$	$\lambda=1$
2.5	0.7611	2.1978	1.8446	0.1721	2.2447	1.0675	0.2046	2.3811	2.4908
2.2	0.8633	2.1368	1.9077	0.2317	2.1969	1.0790	0.1987	2.3389	2.5881
2	0.9370	2.0915	1.9601	0.2822	2.1613	1.1223	0.1949	2.2971	2.6564
1.7	1.0550	2.0146	2.0612	0.3779	2.1002	1.2169	0.1870	2.2364	2.8085
1.5	1.1373	1.9556	2.1511	0.4578	2.0532	1.2685	0.1807	2.1890	2.9477
1.3	1.2227	1.8900	2.2773	0.5530	1.9997	1.3816	0.1729	2.1348	3.1364
1	1.3447	1.7702	2.5402	0.7279	1.9028	1.7068	0.1576	2.0369	3.5945
0.8	1.4188	1.6723	2.9143	0.8660	1.8215	2.2633	0.1433	1.9551	4.1460
0.5	1.4873	1.4754	4.5065	1.0912	1.6542	4.4094	0.4458	1.7872	6.2508

4. Results and discussion

In this portion, the impacts of the relevant parameters upon the non-dimensional outlines are measured. The surface drag forces and HT rate are computed in Table 6.

In general, the Sherwood number is not commonly discussed in the context of HH reactions because it is not as relevant to understanding the underlying kinetics and transport processes. However, in certain cases where mass transfer plays a noteworthy part in

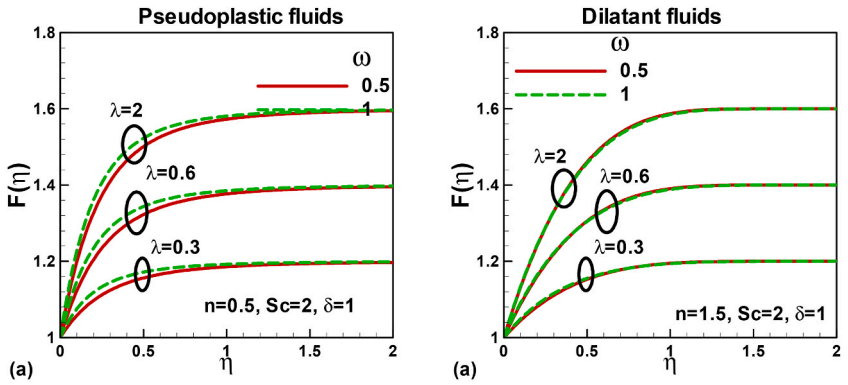

Fig. 2. (a, b): Impacts of velocity ratio and rotation parameters on radial velocity.

the reaction rate, the Sherwood number may be a useful parameter to consider.

The impacts of velocity ratio and rotation parameters upon the dimensionless radial velocity of pseudoplastic and dilatant power-law fluids are presented in Fig. 2 (a, b), respectively. The power-law fluid flows upon a stretching spinning porous disk filled with HH reactions. It is apparent that the dimensionless radial velocity of pseudoplastic and dilatant power-law fluids escalates with an escalation in the velocity ratio and rotation parameter due to the changes in viscosity caused by the increased shear rates and deformation experienced by the fluid.

In fact, pseudoplastic fluids are described by a reduction in viscosity with escalating shear rate, while dilatant fluids exhibit an escalating viscosity with a reducing shear rate. The power-law fluid model describes the viscosity of such fluids as a shear rate, flow behavior index (n), and consistency index (K), where n represents the degree of pseudoplasticity or dilatancy. As the rotation parameter increases, the fluid experiences more shear and deformation, resulting in an escalation in the shear rate and a corresponding increase in the dimensionless radial velocity. The rotation of the disk has a considerable impact upon the dimensionless radial velocity of the fluid, with higher rotation rates resulting in higher values of the dimensionless radial velocity.

The understanding of these effects can provide valuable insights into the behavior of complex fluids in industrial applications and inform the design and optimization of chemical reactors and heat exchangers.

The impacts of velocity ratio and rotation parameters on the non-dimensional azimuthal velocity of pseudoplastic and dilatant nanofluids are exhibited in Fig. 3 (a, b). For a pseudoplastic power-law fluid, the dimensionless azimuthal velocity decreases as the velocity ratio increases. Physically, as the stretching velocity at the disk surface increases, the shear stress on the fluid also increases, leading to a decrease in viscosity. This decrease in viscosity causes a diminution in the azimuthal velocity. On the other hand, the dimensionless azimuthal velocity of a pseudoplastic power-law fluid increases with increasing rotation parameters, such as the disk rotation and the fluid rotation. This is because of the reason that the rotation of the disk and fluid generates centrifugal forces that cause the fluid to progress outwards, resulting in an escalation in the azimuthal velocity. It is essential to notice that, for a dilatant power-law fluid, the dimensionless azimuthal velocity also decreases as the velocity ratio increases. However, an escalation in the stretchable velocity at the disk surface causes an escalation in the viscosity of the fluid, resulting in a reduction in the azimuthal velocity. Similar to the pseudoplastic fluid case, the dimensionless azimuthal velocity of a dilatant power-law fluid escalates with escalating rotation parameters. This is because of the reason that the rotation of the disk and fluid generates centrifugal forces that cause the fluid to progress outwards, resulting in an escalation in the azimuthal velocity.

Fig. 4 (a, b) illustrate the impact of MHD and n on the dimensionless axial velocity of pseudoplastic and dilatant power-law fluids. For a pseudoplastic power-law fluid, the dimensionless axial velocity escalates with increasing magnetic field strength. This is for the

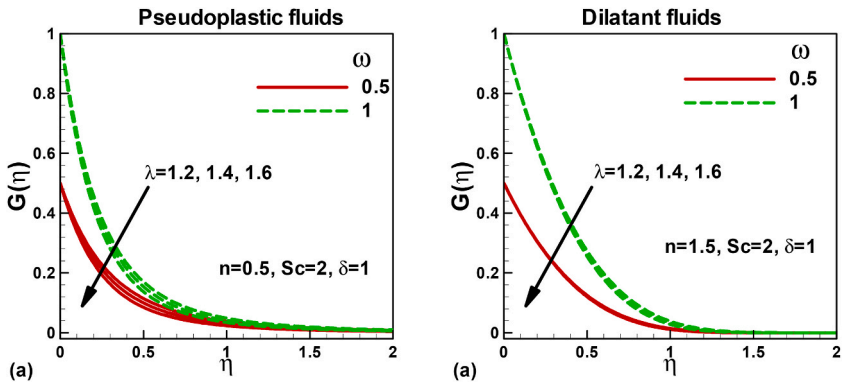

Fig. 3. (a, b): Impacts of velocity ratio and rotation parameters on azimuthal velocity.

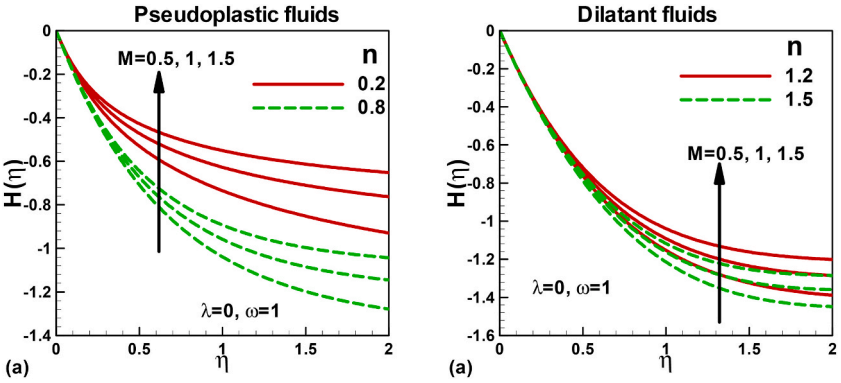

Fig. 4. (a, b): Impacts of magnetic field and power-law index on axial velocity.

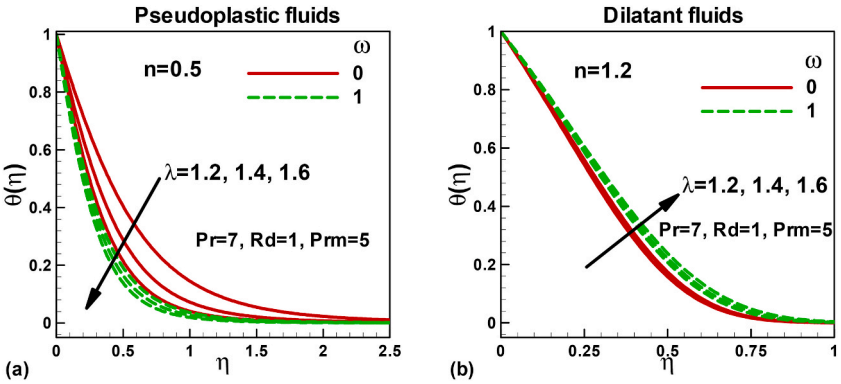

Fig. 5. (a, b): Impacts of velocity ratio and rotation parameters on temperature.

reason that the MHD generates Lorentz forces that perform on the fluid, causing it to accelerate in the axial direction. The magnitude of the Lorentz forces depends on the power of the magnetic field, the fluid's electrical conductivity, and the velocity. The impact of *n* upon the dimensionless axial velocity of a pseudoplastic fluid depends on the specific estimations of the *n*. In general, as the *n* rises, the fluid's shear stress and viscosity also rise, which can lead to a decay in the axial velocity. For a dilatant power-law fluid, the axial velocity also reduces with a growing *n*. Physical justification of this reasonis that the higher power-law index corresponds to a fluid's higher shear stress and viscosity, which reduces the axial velocity.

The consequences of velocity ratio and rotation parameter upon the non-dimensional temperature of pseudoplastic and dilatant power-law fluids over a stretching spinning porous disk are presented in Fig. 5 (a, b). It is exposed that, for a pseudoplastic power-law fluid, the dimensionless temperature decreases with increasing velocity ratio and rotation parameter. Physical reason behind this behavior is that the higher velocity ratio and rotation parameter lead to increased shear rates and therefore increased heat generation due to viscous dissipation, resulting in a decrease in temperature.

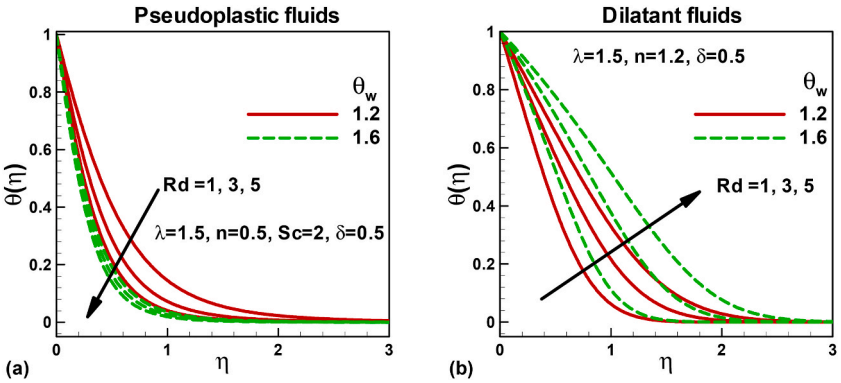

Fig. 6. (a, b): Impacts of radiation and temperature ratio parameters on the temperature.

For a dilatant power-law fluid, the dimensionless temperature escalates with increasing velocity ratio and rotation parameter. Physical justification behind this result is the higher velocity ratio and rotation parameter lead to increased shear rates and therefore increased heat generation due to viscous dissipation, resulting in an increase in temperature.

For a pseudoplastic power-law fluid, the dimensionless temperature reduces with increasing radiation and wall temperature ratio, as indicated in Fig. 6 (a). Physically, the higher radiation and wall temperature ratio leads to increased heat loss from the fluid, which reduces its temperature. Additionally, for pseudoplastic fluids, a higher wall temperature ratio can result in increased viscosity, which can further reduce the temperature due to increased viscous dissipation.

For a dilatant power-law fluid, the dimensionless temperature grows with increasing radiation and wall temperature ratio, as displayed in Fig. 6 (b). This is because the higher radiation and wall temperature ratio leads to increased heat absorption by the fluid, which increases its temperature. Additionally, for dilatant fluids, a higher wall temperature ratio can result in increased viscosity, which can further increase the temperature due to increased viscous dissipation.

Fig. 7 (a, b) disclose that the non-dimensional concentration increases with modified Prandtl Pr_m and Schmidt Sc numbers for both pseudoplastic and dilatant fluids over a stretching spinning porous disk. It is well known that the Pr_m signifies the relation of the momentum to the thermal diffusivities, while the Sc represents the relation of the momentum to the mass diffusivities. In general, higher estimations of Pr_m and Sc agreed to a higher momentum or mass transfer rate, respectively. For pseudoplastic power-law fluids and dilatant fluids, the diffusion process is enhanced owing to the non-Newtonian nature of the fluid. As the fluid flows over the porous disk, the concentration gradients at the fluid-porous interface drive the diffusion of species across the BL, leading to an escalation in the concentration in the bulk of the fluid. Higher values of Pr_m and Sc increases the momentum or mass transfer rate, respectively, which leads to a more efficient diffusion process and a faster increase in the concentration of the species in the bulk of the fluid. Hence, the dimensionless concentration of both pseudoplastic and dilatant fluids increases with increasing Pr_m and Sc.

In a system with homogeneous and heterogeneous reactions involving power-law fluids, the dimensionless concentration of the species is influenced by the reaction parameters K_1 and K_2. Homogeneous reactions occur uniformly throughout the fluid, while heterogeneous reactions occur at the fluid-porous interface. The impacts of HH reaction parameters upon the dimensionless concentration are portrayed in Fig. 8 (a, b). It is demonstrated that the dimensionless concentration of the species decreases depending on the nature of the homogeneous reaction. An endothermic reaction will decay the temperature, which escalates the viscosity and reduces the mass transport coefficient, thereby decreasing the rate of diffusion and the concentration of the species. In general, the dimensionless concentration is influenced by the activation energy, the rate of the reaction, and the heat of the reaction. A higher activation energy will lessen the rate of reaction, which in turn will reduce the concentration of the species. The heat of the reaction can also affect the temperature and viscosity of the fluid, which can further impact the diffusion process and the concentration of the species.

In a system with non-Newtonian power-law fluids flowing upon a spinning porous disk, the dimensionless radial and tangential skin friction is influenced by the velocity ratio, magnetic field, and power-law index n. This is explained in Fig. 9 (a, b) for both cases. The skin friction measures the shear stress used by the fluid on the surface of the disk and is expressed by the dimensionless shear stress. As the n rises, the shear-thinning case of the fluid becomes more prominent, leading to a decrease in the skin friction coefficient. For $n = 1$, the skin friction coefficient is constant. However, for $n < 1$, the skin friction coefficient decays as the n reduces. The dimensionless skin friction decays with a growing velocity ratio. This is because as the velocity ratio escalates, the radial velocity close to the disc's surface disk increases, which reduces the thickness of the BL and hence the shear stress exerted upon the surface of the disk. As the magnetic parameter escalates, the skin friction coefficient increases. This is because the magnetic field persuades an electric current in the fluid, which in turn generates a Lorentz force that opposes the fluid flow. This results in an escalation in the shear stress at the wall, leading to a rise in the skin friction coefficient. Overall, the skin friction coefficient is affected by the n, velocity ratio, and magnetic parameter. These parameters can be optimized to minimize the skin friction coefficient, thereby reducing the energy required to transport the fluid.

A Nusselt number is a non-dimensional number that relates the convective HT at a boundary to the conductive HT in the fluid. The Nusselt number is affected by several factors, including the Prandtl number, radiation parameter, and temperature ratio, as shown in Fig. 10 (a, b). The radiation parameter represents the significance of radiative HT comparative to convective HT. As the radiation parameter increases, radiative heat transfer becomes more significant and boosts the Nusselt number for both power-law fluids. In general, the effect of radiation is more pronounced for high-temperature systems or for systems with high-emissivity surfaces. The temperature ratio is delineated as the ratio of the surface temperature of the boundary to the free stream temperature. As the temperature ratio increases, the HT from the surface to the fluid develops more efficiently, and the Nusselt number increases in both cases. For pseudoplastic, the power-law index is less than 1, which means that the apparent viscosity decays as the shear rate rises. This consequences in a decline in the thermal BL thickness and an escalation in the convective HT coefficient. For dilatant fluids, the Prandtl number is typically higher than for Newtonian fluids. This is because the effective thermal diffusivity is escalated owing to the declination in the thermal BL thickness caused by the shear thinning case of the fluid. Therefore, for pseudoplastic and dilatant fluids, the combination of the shear thinning behavior and the higher Prandtl number precedents an escalation in the convective HT coefficient and hence an escalation in the Nusselt number. This escalation in convective HT can result in more efficient HT and can be useful in industrial processes where HT is critical.

The Nusselt number represents the convective HT coefficient and is delineated as the relation of convective HT to conductive HT. In the instance of non-Newtonian power-law fluids, the Nusselt number can be influenced by the n, velocity ratio, and magnetic parameters in Fig. 11 (a, b). The parameter n measures the shear-thinning or shear-thickening performances of the fluid. As the parameter n decays, the apparent viscosity decreases, resulting in a reduction in the thermal BL thickness and an escalation in the convective HT coefficient. Therefore, as the parameter n decreases, the Nusselt number generally rises. The velocity ratio indicates the relation of the

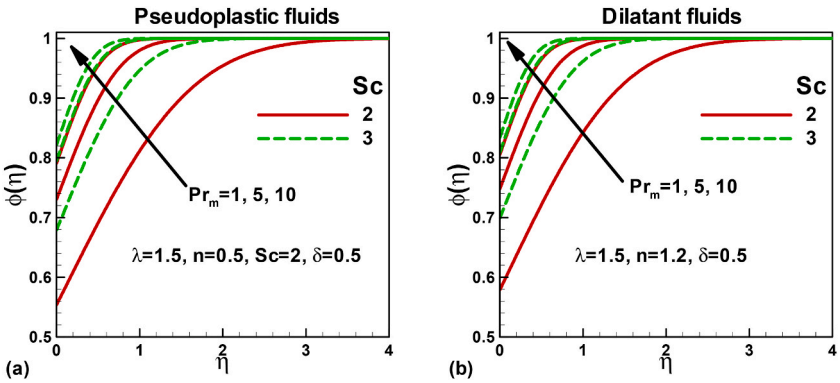

Fig. 7. (a, b): Impacts of modified Prandtl and Schmidt numbers upon the concentration.

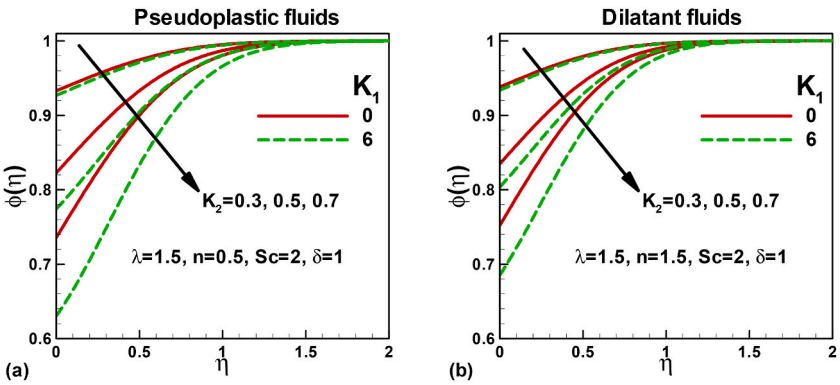

Fig. 8. (a, b): Impacts of HH reaction parameters on dimensionless concentration.

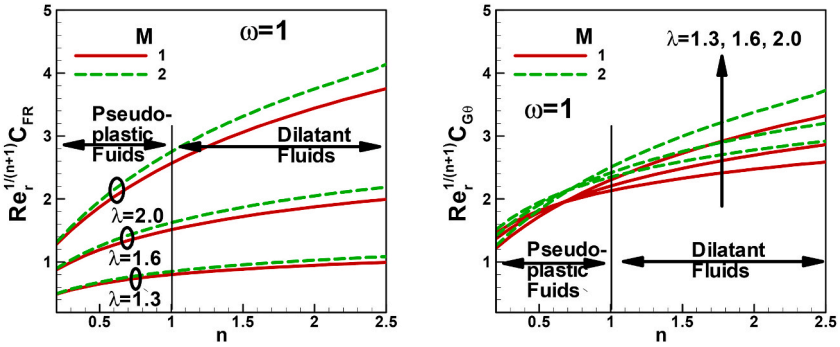

Fig. 9. (a, b): Alteration of skin friction with the power-law index for diverse estimations of velocity ratio and magnetic parameters.

velocity of the rotating disk to the velocity of the free stream. As the velocity ratio increases, the fluid experiences higher levels of shear, which escalates the convective HT coefficient. Therefore, as the velocity ratio escalates, the Nusselt number generally grows. The magnetic parameters refer to the power of the magnetic field and the magnetic properties of the fluid. With a magnetic field, the flow behavior of the non-Newtonian fluid can be modified, which can affect the convective HT coefficient. Generally, the magnetic field can lead to an increase in the convective HT coefficient, particularly for fluids with higher magnetic susceptibility. Therefore, as the magnetic parameters increase, the Nusselt number generally escalates for pseudoplastic fluids.

5. Conclusion

Theoretical exploration of HT in a stagnant power-law fluid flow upon a stretchable spinning porous disk filled with HH reactions involves the examination of the HT mechanisms and fluid dynamics in this system. The theoretical model for this system considers a power-law fluid flowing upon a spinning porous disk, which is stretched in the radial direction. The porous disk is filled with a HH

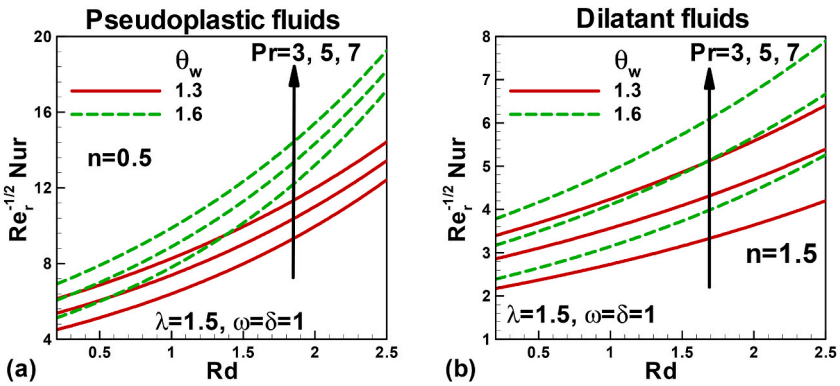

Fig. 10. (a, b): Alteration of Nusselt number with radiation parameter for diverse fluids and temperature ratio.

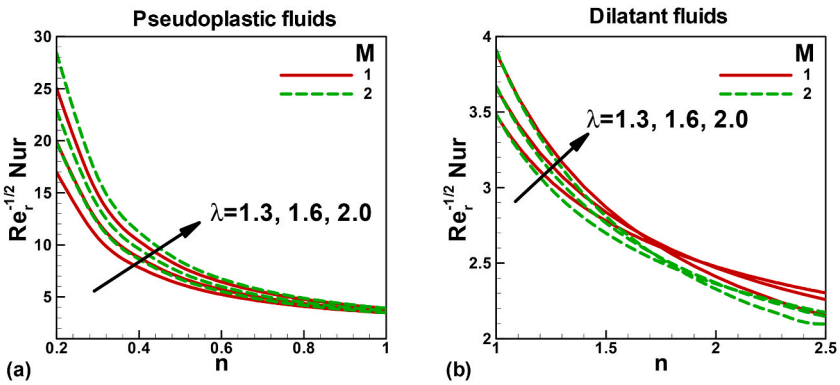

Fig. 11. (a, b): Alteration of Nusselt number with power-law index *n* for diverse estimations of velocity ratio and magnetic parameters.

chemical reaction that generates or absorbs heat, depending on the reaction conditions. The study utilizes a theory developed by Chaudhary and Merkin, which is modified to address the present problem of a stretching sheet in a power-law fluid. The focus is on examining the impact of equal diffusivities for reactant and auto catalyst in the stagnant-point BL flow. The study starts by modeling the fluid flow using the continuity, momentum, and energy conservation equations, which are then handled numerically via assumed BCs. The momentum conservation equation is modified to account for the impacts of porosity and the stretching and spinning of the disk. The key discoveries are abridged as given:

- The dimensionless radial velocity of both power-law fluids rises with a rise in the velocity ratio and rotation parameters.
- The dimensionless azimuthal velocity of both power-law fluids rises with escalating rotation parameters but decays with the velocity ratio.
- For both power-law fluids, the dimensionless axial velocity grows with growing magnetic field power while decaying with an escalation in the power-law index.
- The dimensionless temperature decreases for the pseudoplastic power-law fluid and escalates for the dilatant power-law fluid as the velocity ratio, rotation, radiation, and wall temperature ratio parameters increase.
- The dimensionless concentration increases with Schmidt and modified Prandtl numbers for both power-law fluids over a stretching spinning porous disk.
- The HH reaction parameters decline the concentration of power-law fluids.
- The dimensionless skin friction of both power-law fluids decreases with increasing velocity ratio and magnetic parameters. However, it escalates with escalating power-law index.
- The Prandtl number, velocity ratio, temperature ratio, and magnetic and radiation parameters enhance the HT rate.

Future work

This study analyzes the HT features in an MHD stagnant flow of power-law fluid caused by a spinning disk that is stretched and saturated in a porous medium; nonetheless influence of another viscoelastic fluid model along with effects of nonlinear thermal radiation along with the gyrotactic microorganism well-thought-out in the near future.

Author statement

Zhihong He: Analysis and Investigation.
Muhammad Bilal Arain: Writing an original Draft.
Usman: Writing, Reviewing, and Editing.
W. A. Khan: Software, Methodology.
Ali Rashash R Alzahrani: Data analysis and Management.
Taseer Muhammad: Conceptualization.
A.S. Hendy: Visualization.
Mohamed R. Ali: Validation.

Declaration of competing interest

We wish to confirm that there are no known conflicts of interest associated with this publication, and there has been no significant financial support for this work that could have influenced its outcome.

Data availability

Data will be made available on request.

Acknowledgment

The authors extend their appreciation to the Deanship of Scientific Research at King Khalid University, Abha, Saudi Arabia for funding this work through Large Groups Project under grant number RGP.2/492/44.

References

[1] A.B. Metzner, Heat transfer in non-Newtonian fluids, in: Advances in Heat Transfer, vol. 2, Elsevier, 1965, pp. 357–397, https://doi.org/10.1016/S0065-2717(08)70264-8.
[2] M. Mustafa, A. Mushtaq, T. Hayat, A. Alsaedi, Model to study the nonlinear radiation heat transfer in the stagnation-point flow of power-law fluid, Int. J. Numer. Methods Heat Fluid Flow 25 (5) (2015) 1107–1119, https://doi.org/10.1108/HFF-05-2014-0147.
[3] Usman, A. Ghaffari, T. Muhammad, I. Mustafa, Heat transfer enhancement in a power-law nanofluid flow between two rotating stretchable disks, Pramana 96 (1) (2022) 40, https://doi.org/10.1007/s12043-021-02272-0.
[4] R. Cortell, A note on magnetohydrodynamic flow of a power-law fluid over a stretching sheet, Appl. Math. Comput. 168 (1) (2005) 557–566, https://doi.org/10.1016/j.amc.2004.09.046.
[5] T. Von Karman, Uber laminar and turbulent reibung, Z. Angew. Math. Mech. (1921) 233–235, https://doi.org/10.1002/zamm.19210010401.
[6] W.G. Cochran, The flow due to a rotating disc, in: Mathematical Proceedings of the Cambridge Philosophical Society, vol. 30, Cambridge University Press, 1934, July, pp. 365–375, https://doi.org/10.1017/S0305004100012561, 3.
[7] K. Sarada, R.J.P. Gowda, I.E. Sarris, R.N. Kumar, B.C. Prasannakumara, Effect of magnetohydrodynamics on heat transfer behaviour of a non-Newtonian fluid flow over a stretching sheet under local thermal non-equilibrium condition, Fluid 6 (8) (2021) 264, https://doi.org/10.3390/fluids6080264.
[8] J. Ahmed, M. Khan, L. Ahmad, Stagnation point flow of Maxwell nanofluid over a permeable rotating disk with heat source/sink, J. Mol. Liq. 287 (2019), 110853, https://doi.org/10.1016/J/MOLLIQ.2019.04.130.
[9] S. Dinarvand, A.M. Nejad, Off-centered stagnation point flow of an experimental-based hybrid nanofluid impinging to a spinning disk with low to high non-alignments, Int. J. Numer. Methods Heat Fluid Flow 32 (8) (2021) 2799–2818, https://doi.org/10.1108/HFF-09-2021-0637.
[10] M. Yaseen, S.K. Rawat, U. Khan, A.S. Negi, M. Kumar, E.S.M. Sherif, I. Pop, Inspection of unsteady buoyancy and stagnation point flow incorporated by Ag- TiO2 hybrid nanoparticles towards a spinning disk with Hall effects, Case Stud. Therm. Eng. (2023), 102889, https://doi.org/10.1016/j.csite.2023.102889.
[11] K. Millsaps, K. Pohlhausen, Heat transfer by laminar flow from a rotating plate, J. Aeronaut. Sci. 19 (2) (1952) 120–126, https://doi.org/10.2514/8.2175.
[12] M.D. Shamshuddin, F. Mabood, A numerical model for analysis of binary chemical reaction and activation energy of thermo solutal micropolar nanofluid flow through permeable stretching sheet: nanoparticle study, Phys. Scripta 96 (7) (2021), 075206, https://doi.org/10.1088/1402-4896/abf794.
[13] r. Agarwal, An analytical study of non-Newtonian visco-inelastic fluid flow between two stretchable rotating disks, Palestine J. Mathemat. 11 (2022).
[14] G. Gupta, P. Rana, Comparative study on Rosseland's heat flux on three- dimensional MHD Stagnation-point multiple slip flow of ternary hybrid nanofluid over a stretchable rotating disk, Mathematics 10 (18) (2022) 3342, https://doi.org/10.3390/math10183342.
[15] N. Vijay, K. Sharma, Dynamics of stagnation point flow of Maxwell nanofluid with combined heat and mass transfer effects: a numerical investigation, Int. Commun. Heat Mass Tran. 141 (2023), 106545, https://doi.org/10.1016/j.icheatmasstransfer.2022.106545.
[16] M.I. Khan, M. Waqas, T. Hayat, A. Alsaedi, A comparative study of Casson fluid with homogeneous-heterogeneous reactions, J. Colloid Interface Sci. 498 (2017) 85–90, https://doi.org/10.1016/j.jcis.2017.03.024.
[17] M. Gholinia, K. Hosseinzadeh, H. Mehrzadi, D.D. Ganji, A.A. Ranjbar, Investigation of MHD Eyring–Powell fluid flow over a rotating disk under effect of homogeneous–heterogeneous reactions, Case Stud. Therm. Eng. 13 (2019), 100356, https://doi.org/10.1016/j.csite.2018.11.007.
[18] M. Imtiaz, F. Mabood, T. Hayat, A. Alsaedi, Homogeneous-heterogeneous reactions in MHD radiative flow of second grade fluid due to a curved stretching surface, Int. J. Heat Mass Tran. 145 (2019), 118781, https://doi.org/10.1016/j.ijheatmasstransfer.2019.118781.
[19] P. Sreedevi, P. Sudarsana Reddy, M.A. Sheremet, Impact of homogeneous– heterogeneous reactions on heat and mass transfer flow of Au–Eg and Ag–Eg Maxwell nanofluid past a horizontal stretched cylinder, J. Therm. Anal. Calorim. 141 (2020) 533–546, https://doi.org/10.1007/s10973-020-09581-3.
[20] W.A. Khan, I.M. Pop, Effects of Homogeneous–Heterogeneous Reactions on the Viscoelastic Fluid Toward a Stretching Sheet, J. Heat Transfer 134 (6) (2012), 064506, https://doi.org/10.1115/1.4006016.
[21] N. Bachok, A. Ishak, I. Pop, On the stagnation-point flow towards a stretching sheet with homogeneous–heterogeneous reactions effects, Commun. Nonlinear Sci. Numer. Simulat. 16 (11) (2011) 4296–4302, https://doi.org/10.1016/j.cnsns.2011.01.008.
[22] P.K. Kameswaran, S. Shaw, P. Sibanda, P.V.S.N. Murthy, Homogeneous–heterogeneous reactions in a nanofluid flow due to a porous stretching sheet, Int. J. Heat Mass Tran. 57 (2) (2013) 465–472, https://doi.org/10.1016/j.ijheatmasstransfer.2012.10.047.
[23] S. Shaw, P.K. Kameswaran, P. Sibanda, Homogeneous-heterogeneous reactions in micropolar fluid flow from a permeable stretching or shrinking sheet in a porous medium, Bound. Value Probl. 2013 (1) (2013) 77, https://doi.org/10.1186/1687-2770-2013-77.
[24] Z. Abbas, M. Sheikh, I. Pop, Stagnation-point flow of a hydromagnetic viscous fluid over stretching/shrinking sheet with generalized slip condition in the presence of homogeneous–heterogeneous reactions, J. Taiwan Inst. Chem. Eng. 55 (2015) 69–75, https://doi.org/10.1016/j.jtice.2015.04.001.

[25] M. Sheikh, Z. Abbas, Homogeneous–heterogeneous reactions in stagnation point flow of Casson fluid due to a stretching/shrinking sheet with uniform suction and slip effects, Ain Shams Eng. J. 8 (3) (2017) 467–474, https://doi.org/10.1016/j.asej.2015.09.010.
[26] T. Hayat, A. Kiran, M. Imtiaz, A. Alsaedi, Effect of homogeneous–heterogeneous reactions in stagnation point flow of third grade fluid past a variable thickness stretching sheet, Neural Comput. Appl. (2017), https://doi.org/10.1007/s00521-017-2913-z.
[27] S. Jain, P. Gupta, Numerical study of water-based carbon nanotubes' nanofluid flow over a nonlinear inclined 3-D stretching sheet for homogeneous–heterogeneous reactions with porous media, Lecture Notes in Electrical Engineering (2018) 633–649, https://doi.org/10.1007/978-981-13-1642-5_56.
[28] N.S. Anuar, N. Bachok, N.M. Arifin, H. Rosali, Homogeneous-heterogeneous reactions in the stagnation-point flow and heat transfer of nanofluids over an exponentially stretching/shrinking sheet with stability analysis, in: Proceedings of the International Conference on Mathematical Sciences and Technology 2018 (MATHTECH2018): Innovative Technologies for Mathematics & Mathematics for Technological Innovation, 2019, https://doi.org/10.1063/1.5136446.
[29] J.H. Merkin, A model for isothermal homogeneous-heterogeneous reactions in boundary-layer flow, Math. Comput. Model. 24 (1996) 125–136, https://doi.org/10.1016/0895-7177(96)00145-8.
[30] N.A. Latiff, M.J. Uddin, A.M. Ismail, Stefan blowing effect on bioconvective flow of nanofluid over a solid rotating stretchable disk, Propul. Power Res. 5 (4) (2016) 267–278, https://doi.org/10.1016/j.jppr.2016.11.002.
[31] F. Tuz Zohra, M.J. Uddin, M.F. Basir, A.I.M. Ismail, Magnetohydrodynamic bio-nano-convective slip flow with Stefan blowing effects over a rotating disc, Proc. Inst. Mech. Eng., Part N: J. Nanomaterials, Nanoengineering Nanosystems 234 (3–4) (2020) 83–97, https://doi.org/10.1177/239779141988158.
[32] M.J. Uddin, P. Rana, S. Gupta, M.N. Uddin, Bio-nanoconvective micropolar fluid flow in a Darcy porous medium past a cone with second-order slips and stefan blowing: FEM solution, Iranian J. Sci. Technol. Transact. Mechanical Eng. (2023) 1–15, https://doi.org/10.1007/s40997-023-00626-0.
[33] M. Turkyilmazoglu, Nanofluid flow and heat transfer due to a rotating disk, Comput. Fluid 94 (2014) 139–146, https://doi.org/10.1016/j.compfluid.2014.02.009.
[34] N. Bachok, A. Ishak, I. Pop, Flow and heat transfer over a rotating porous disk in a nanofluid, Physica B 406 (2011) 1767–1772, https://doi.org/10.1016/j.physb.2011.02.024.
[35] N. Kelson, A. Desseaux, Note on porous rotating disk flow, ANZIAM J. 42 (2000) C837–C855, https://doi.org/10.21914/anziamj.v42i0.624.
[36] P. Mitschka, J. Ulbricht, Nicht-Newtonsche Flüssigkeiten IV. Strömung Nicht-Newtonscher Flüssigkeiten Ostwald-de-Waeleschen Ttyps in der Umgebung Rotierender Drehkegel und Scheiben, N. Collect Czech Chem. Commun. 30 (1965) 2511–2526, https://doi.org/10.1135/cccc19652511.
[37] H.I. Andersson, E. De Korte, R. Meland, Flow of a power-law fluid over a rotating disk revisited, Fluid Dynam. Res. 28 (2001) 75–88, https://doi.org/10.1016/S0997-7546(02)01184-6.
[38] C.Y. Ming, L. Zheng, X. Zhang, Steady flow and heat transfer of the power-law fluid over a rotating disk, Int. Commun. Heat Mass Tran. 38 (2011) 280–284, https://doi.org/10.1016/j.icheatmasstransfer.2010.11.013.
[39] Usman, P. Lin, A. Ghaffari, Steady flow and heat transfer of the power-law fluid between two stretchable rotating disks with non-uniform heat source/sink, J. Therm. Anal. Calorim. (2020), https://doi.org/10.1007/s10973-020-10142-x.
[40] H.B. Keller, A new difference scheme for parabolic problems, in: Numerical Solutions of Partial Differential Equations, Academic Press, New York, 1970, https://doi.org/10.1016/B978-0-12-358502-8.50014-1.
[41] T. Cebeci, P. Bradshaw, Physical and Computational Aspects of Convective Heat Transfer, Springer-Verlag, New York, 1988.
[42] A. Ishak, R. Nazar, I. Pop, Post-stagnation-point boundary layer flow and mixed convection heat transfer over a vertical, linearly stretching sheet, Arch. Mech. 60 (2008) 303–322.